JOURNAL OF AIRCRAFT
Vol. 34, No. 6, November–December 1997

Method for the Constrained Design of Natural Laminar Flow Airfoils

Bradford E. Green* and John L. Whitesides†
George Washington University, Hampton, Virginia 23681-0001
and
Richard L. Campbell‡ and Raymond E. Mineck§
NASA Langley Research Center, Hampton, Virginia 23681-0001

An automated iterative design method has been developed by which an airfoil with a substantial amount of natural laminar flow can be designed while maintaining other aerodynamic and geometric constraints. Drag reductions have been realized using the design method over a range of Mach numbers, Reynolds numbers, and airfoil thicknesses. The key features of the method are the compressible linear stability analysis code used to calculate *N*-factors; the ability to calculate a target *N*-factor distribution that forces the flow to undergo transition at the desired location; the target pressure/*N*-factor relationship that is used to modify target pressures to produce the desired *N*-factor distribution; and its ability to design airfoils to meet lift, pitching moment, thickness, and leading-edge radius constraints while also being able to meet the natural laminar flow constraint.

Nomenclature

A = relaxation factor for N-factor design method
a = amplitude of Tollmien–Schlichting waves
C_p = pressure coefficient
c_l = section lift coefficient
c_m = pitching moment coefficient
N = N-factor
x = nondimensional distance along chord of airfoil

Subscripts
a = analysis
cp = control point
j = airfoil station
stag = stagnation point
T = target

Introduction

SINCE the advent of powered flight, drag reduction has been a major issue in airplane design. For example, reductions in drag allow airplanes to operate more efficiently by using less fuel, which results in reduced operating costs and smaller, quieter engines. The design of airplanes with bigger payloads and longer ranges is also possible when drag is reduced.

There have been many concepts to reduce airplane drag. Since the 1930s, there has been great interest in designing airfoils and wings for natural laminar flow (NLF) to reduce viscous drag. In addition, supercritical wings were developed to reduce the wave drag on airplanes. Moreover, the use of winglets on airplanes today demonstrates an approach to reduce induced drag. This paper presents a design method for reducing drag through the design of NLF airfoils.

Received Sept. 16, 1996; revision received May 20, 1997; accepted for publication June 2, 1997.

*Graduate Research Scholar Assistant, Joint Institute for Advancement of Flight Sciences, M/S 499. Student Member AIAA.
†Professor of Engineering and Applied Science, Joint Institute for Advancement of Flight Sciences, M/S 269. Associate Fellow AIAA.
‡Research Engineer, M/S 499. Associate Fellow AIAA.
§Research Engineer, M/S 499.

Method

This new design method[1] combines proven computational fluid dynamics (CFD) analysis and design codes with a new target pressure design technique. The computational tools, which were readily available, have been coupled together in modular form so that any one of them can be replaced by another preferred code.

A flowchart of the method is shown in Fig. 1. This flowchart represents the process by which a single surface is designed for natural laminar flow. In cases where laminar flow is desired on both surfaces, this method is applied successively to each surface.

After generating a grid for the initial airfoil, the GAUSS2 Euler solver,[2–4] coupled with a turbulent boundary-layer method,[5] is used to calculate the pressure distribution of the starting airfoil. Then, a laminar boundary-layer solver[6] is used to calculate the boundary-layer velocity and temperature profiles. These profiles are then used by COSAL,[7] a compressible linear stability analysis code, to calculate the N-factors for the current airfoil. The N-factors, which are proportional to the growth of the boundary-layer instabilities, are described by the following equation:

$$N = \ell n(a/a_0) \tag{1}$$

In this equation, a is at a point in the flow within the boundary layer, and a_0 is the amplitude at the beginning of the instability region. According to Mack,[8] a can represent any flow variable. The N-factors have been correlated with transition, with the transition N-factor being between 8–15, depending on whether the correlation was made through wind-tunnel tests or in-flight experiments.

Using the current pressures and N-factors, the target pressure design module then calculates a target pressure distribution that increases the amount of laminar flow over the airfoil. Once the target pressures are known, the CDISC airfoil design method[9] then iteratively designs a new airfoil. While using the airfoil design method, the target pressures for the design are

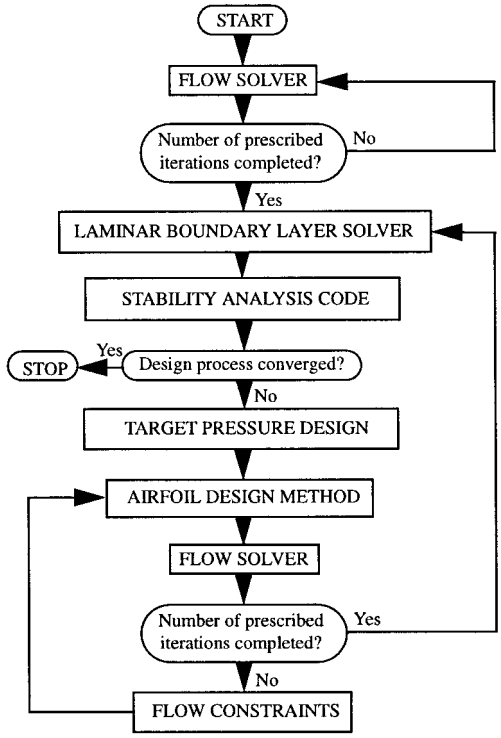

Fig. 1 Flowchart of the NLF airfoil design method.

modified in the flow constraints module so that the lift and pitching moment constraints are achieved.

After designing a new airfoil, the boundary-layer profiles are calculated once again by the laminar boundary-layer solver, so that the stability analysis code can calculate the N-factors of the new airfoil. The method will continue to iterate through these steps until the constraints are satisfied, or until the prescribed number of iterations is achieved. This design method is fully automated and requires only four input files to be specified prior to designing a new airfoil.

This method can be used to design a new airfoil in as few as 10 CPU hours using a Silicon Graphics Indigo2 workstation. The stability analysis code is the most expensive code in the design process, taking approximately 60% of the total CPU time.

Target Pressure Distribution

After choosing an initial airfoil, the pressure distribution of the airfoil is calculated using the flow solver, and the N-factor envelope of the airfoil is calculated using the laminar boundary-layer solver and the stability analysis code. Then, from the current pressure and N-factor distributions, a target pressure distribution is calculated that meets all of the aerodynamic constraints. The module labeled target pressure design in Fig. 1 is responsible for calculating this new target pressure distribution. Figure 2 shows a detailed flowchart of how the target pressure design module calculates the new target pressures. Each of the components in this flowchart will now be discussed.

Target N-Factor Distribution

Once the analysis N-factor distribution has been calculated by the stability analysis code, a target N-factor distribution must be prescribed (Fig. 2). This target N-factor distribution must force the flow to undergo transition at the desired location.

To calculate the target N-factor distribution, four control points ($x_{cp,1}$, $x_{cp,2}$, $x_{cp,3}$, and $x_{cp,4}$) are specified (Fig. 3). The first control point is located at the point where the analysis N-factors first become greater than N-factor level $N_{cp,1}$. Ahead of the

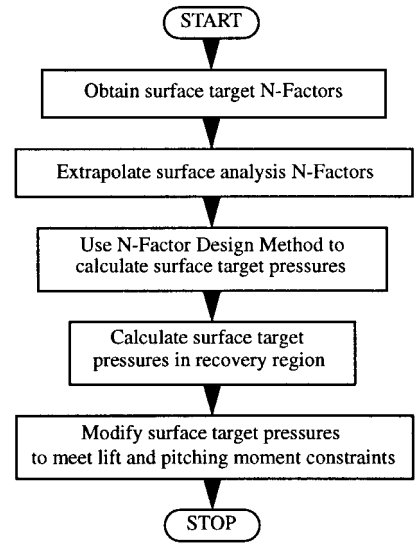

Fig. 2 Flowchart of the target pressure design module.

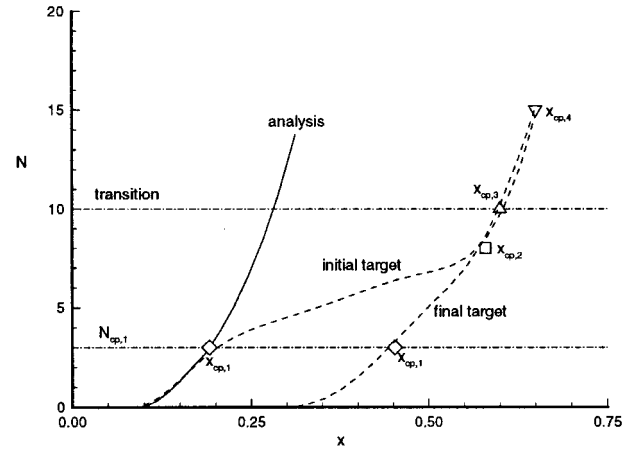

Fig. 3 Two typical target N-factor distribution with control points.

first control point, the analysis N-factors are kept as the target N-factors. Beyond this point, the other control points and their N-factor levels are used to calculate the target N-factors. This is done by interpolating the control points with a polynomial fit.

The second control point is located at the beginning of a region where the N-factors are forced to grow rapidly to make transition occur. In addition, the location of this control point is such that a buffer region is formed above which the N-factors aren't allowed to grow, so that the flow will not undergo transition at slightly off-design conditions. The third control point is placed at the location of desired transition, while the fourth control point represents the end of the steep N-factor gradient. A nominal transition N-factor of 10 is used in Fig. 3.

The analysis N-factor distribution changes with each iteration. Since the target N-factors are dependent on the analysis N-factor distribution, the target N-factors also change slightly with each iteration. To show how much the target N-factors may change throughout the design process, Fig. 3 shows an initial and a final target N-factor distribution. In Fig. 3, $x_{cp,2} = 0.58$, $x_{cp,3} = 0.60$, $x_{cp,4} = 0.65$, $N_{cp,1} = 3$, $N_{cp,2} = 8$, $N_{cp,3} = 10$, and $N_{cp,4} = 15$. Although these numbers are typical, the exact values of the second and fourth control points are not critical. The key requirement is to have an N-factor growth of about 5–10 in 10% chord to ensure transition without causing laminar separation.

Extrapolation of Analysis *N*-Factors

The stability analysis code can calculate *N*-factors only when the laminar boundary layer is attached. This causes problems if the boundary layer of the current airfoil separates ahead of the fourth control point, $x_{cp,4}$. This creates a problem because the *N*-factor design method discussed in the next section requires an analysis *N*-factor at each station, where target *N*-factors are specified. The second module in Fig. 2 is included to remedy this situation.

Choosing pressure as the flow variable to represent a in Eq. (1) and replacing the log function with a series expansion, it was determined that the change in *N*-factor is proportional to the change in pressure over the surface of the airfoil. The analysis *N*-factors are artificially extended between the point of laminar separation and the fourth control point using linear extrapolation based on the pressures.

***N*-Factor Design Method**

After calculating the target *N*-factor distribution and extrapolating the analysis *N*-factors, the *N*-factor design method calculates a target pressure distribution that moves the analysis *N*-factors toward the target *N*-factors. This method, which is shown as the third module in the flowchart in Fig. 2, is based on the target pressure/*N*-factor relationship previously mentioned. In this method, the change in pressure coefficient required at airfoil station j to move the analysis *N*-factor at j, N_j, toward the target *N*-factor at j, $N_{T,j}$, is

$$\Delta C_{p,j} = A\Delta N_j$$

where

$$\Delta C_{p,j} = C_{p,T,j} - C_{p,a,j}, \qquad \Delta N_j = N_{T,j} - N_j$$

In the preceding equations, A is typically 0.012, $C_{p,T,j}$ is the target pressure at station j, and $C_{p,a,j}$ is the analysis pressure at station j.

To maintain a smooth and continuous target pressure distribution, once $\Delta C_{p,j}$ has been calculated, this change in C_p is applied to all of the stations downstream of j as well. In doing this, the flow downstream of j has been changed and, as a result, it is necessary to modify the analysis *N*-factors downstream. This is done by adding ΔN_j to each of the analysis *N*-factors aft of j. The boundary conditions at the stagnation point are

$$C_{p,T,1} = C_{p,a,1} = C_{p,\text{stag}} \qquad N_{T,1} = N_1 = 0$$

Pressures in the Recovery Region

Once the target pressures have been calculated ahead of the fourth control point, the target pressures in the recovery region are calculated, as indicated by the fourth module on the flowchart in Fig. 2. These target pressures are determined based on scaled values of the analysis pressures in the recovery region of the initial airfoil and a triangular lift increment that is used to modify the pressure distribution to meet the pitching moment constraint.

Meeting the Lift and Pitching Moment Constraints

The target pressures that have been calculated must now be modified to meet the desired lift and pitching moment constraints. This is indicated in the fifth module on the flowchart shown in Fig. 2.

While modifying the target pressures to meet the lift and pitching moment constraints, it is also desired to preserve the pressure gradient in the region where the *N*-factors are being constrained so that laminar flow is not disturbed. To accomplish this, the target pressure distribution is divided into three distinct regions. The leading-edge region extends from the leading edge of the airfoil to the last station where the *N*-factors are zero. The center region extends from the last station where the *N*-factors are zero to the fourth control point. Finally, the recovery region, which is used to meet the pitching moment constraint, extends from the fourth control point to the trailing edge.

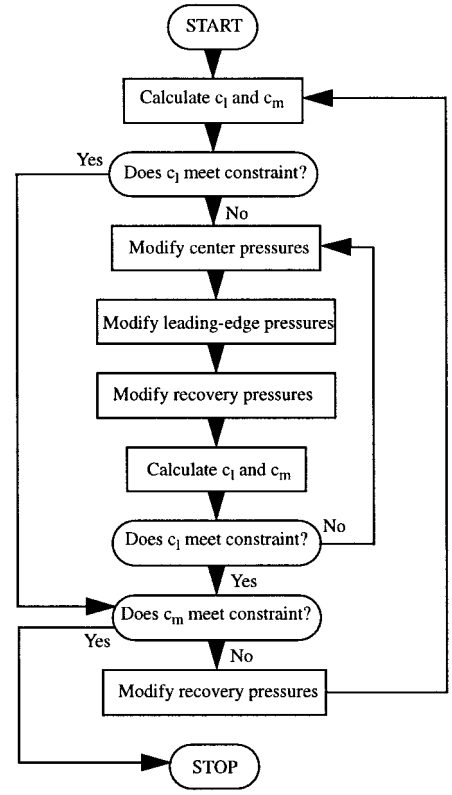

Fig. 4 Flowchart of how the upper surface target pressures are modified to meet the lift and pitching moment constraints.

Figure 4 shows a detailed flowchart of how the target pressures are modified to meet the lift and pitching moment constraints. If the lift constraint is not satisfied, then the pressures in the center region are shifted by an amount that is proportional to the difference between the desired and current lift coefficients. To keep the target pressure distribution smooth, the pressures in the leading-edge region are scaled to meet the new pressures in the center region. The pressures in the recovery region are calculated as discussed in the previous section. This process is repeated until the desired lift coefficient is achieved.

To meet the pitching moment constraint, the pressures in the recovery region are modified by adding a triangular lift increment that is proportional to the difference between the desired pitching moment coefficient and the current pitching moment coefficient. As a result, the target pressures must be modified to once again satisfy the lift constraint. As shown in Fig. 4, this process is repeated until both the lift and pitching moment constraints are achieved.

Two Surface Designs

The current method can be used to design airfoils with laminar flow on one or both surfaces. It is also possible to design the airfoil for various geometric constraints, which include maximum thickness, spar thickness, leading-edge radius, and trailing-edge angle constraints. In these cases, the airfoil geometry is continually scaled by the CDISC airfoil design method so that the airfoil meets the desired geometric constraints. However, when natural laminar flow is desired on both surfaces, it becomes more difficult to maintain some of the geometric constraints while trying to obtain laminar flow on both surfaces. As a result, a tradeoff between geometric con-

straints and the amount of natural laminar flow is often necessary.

Results

The NLF airfoil design method that has been described in the previous sections will now be used to design several airfoils for a variety of flow conditions and constraints. While the initial airfoil used in the first two examples already has a significant amount of laminar flow on both surfaces, the initial airfoil used in the third example does not.

Airfoil for a General Aviation Application

The first airfoil that is presented was designed for the same flow conditions and constraints for which the NLF(1)-0414F airfoil[10] was developed. The aerodynamic design goals for the NLF(1)-0414F airfoil included 70% chord NLF on both surfaces at a Mach number of 0.40, a Reynolds number of 1×10^7, and a lift coefficient of 0.40. In addition, the airfoil was to be 14% thick and have a trailing-edge cruise flap with the pressures in the recovery region being specified to avoid turbulent separation.

The NLF(1)-0414F was developed using the New York University code[11–13] to calculate the pressures of each intermediate airfoil and the SALLY code[14] to perform the stability analysis. Modifications were then made iteratively by hand to the airfoil geometry to give the airfoil the desired characteristics. These characteristics were then experimentally verified in a wind tunnel.

Starting with the NACA 64_1-212 airfoil, a new airfoil was designed by the present NLF airfoil design method that would meet constraints similar to those of the NLF(1)-0414F. The pressures in the recovery region of the new airfoil were designed to prevent the turbulent boundary layer from separating in the event that the flow transitioned at 5% chord. This was done by preventing the Stratford separation criteria[15] from being violated. In addition, to prevent a negative thickness at the trailing edge, the trailing-edge angle was constrained to be greater than 5.7 deg, which is 1% thickness growth in 10% chord from the trailing edge.

Figures 5 and 6 show the upper and lower surface N-factor distributions, respectively, of the NACA 64_1-212 airfoil. In these figures, a transition N-factor of 9 was chosen, which corresponds to wind-tunnel correlations with transition. These plots indicate that the flow on the upper and lower surfaces of the NACA 64_1-212 would transition at about 35 and 50% chord, respectively. In addition, the laminar boundary-layer solver calculated boundary-layer characteristics only to about 50% chord on both surfaces, where laminar separation was then detected. As a result, it was necessary to artificially extend the analysis N-factors to 70% chord, as discussed earlier.

Using the method described previously, a new airfoil was designed to meet the final target N-factor distributions shown in Figs. 5 and 6. These target N-factor distributions were determined from the control points shown in the figures, which constrain transition to occur near 70% chord. The upper and lower surface N-factor distributions of the new airfoil that was designed are also shown in Figs. 5 and 6. From Figs. 5 and 6, one can see that the amount of laminar flow has been increased to 70% chord over both surfaces of the airfoil.

Figure 7 shows a comparison of the pressure distributions of the two airfoils. In general, these pressure distributions appear to be very similar. There is a difference, however, in the leading-edge pressures of the two airfoils. This difference is a result of the fact that the leading-edge radii of the two airfoils are slightly different. The pressures in the midchord region compare very well, although the pressure gradient on the upper surface of the NLF(1)-0414F is more favorable.

All of the constraints imposed in the design of the new airfoil were met. In addition, the design of the new airfoil using the present method took about 14 h of CPU time on a Silicon Graphics Indigo2 workstation with an R4000 processor. Approximately 60% of this time was spent in the stability analysis code, 22% was spent in the flow solver, and less than 1% was spent running the laminar boundary-layer solver and the CDISC airfoil design method. The remaining 16% was used mainly for input and output. For comparison, the development of the NLF(1)-0414F airfoil took approximately one year to complete.

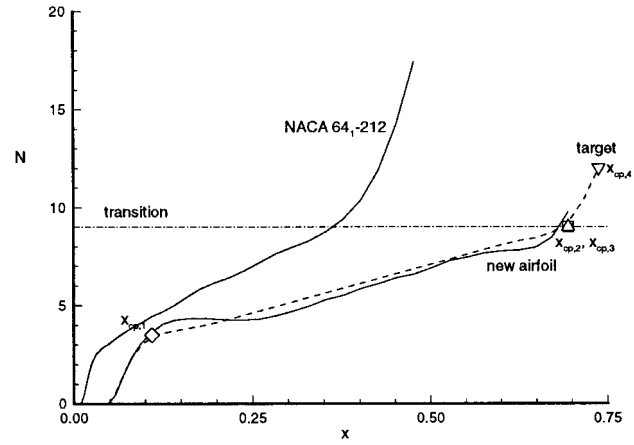

Fig. 5 Comparison of the N-factors on the upper surface of the NACA 64_1-212 and the new airfoil.

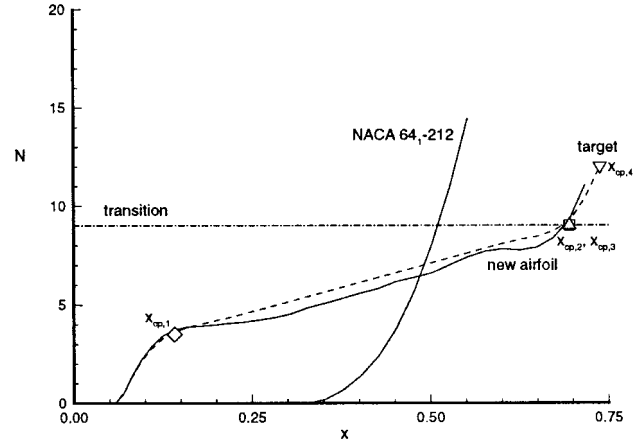

Fig. 6 Comparison of the N-factors on the lower surface of the NACA 64_1-212 and the new airfoil.

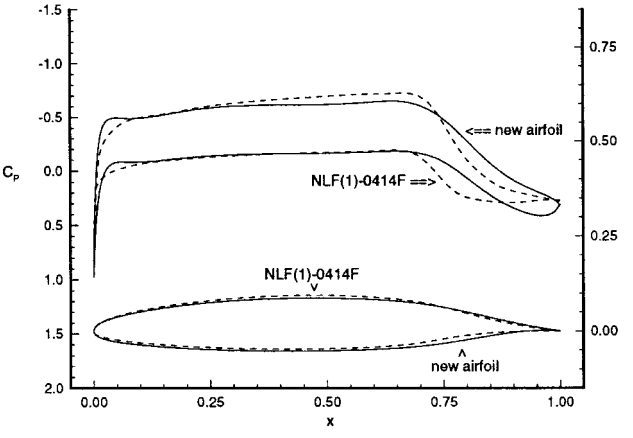

Fig. 7 Comparison of the pressures of the NLF(1)-0414F and the new airfoil at $M = 0.40$, $Re = 1 \times 10^7$, and $c_l = 0.40$.

Airfoil for a Glider Application

Starting from the NACA 64_1-212, an airfoil for a glider application was designed for 65% chord NLF on both surfaces. The airfoil was designed at a Mach number of 0.10, a Reyn-

olds number of 3×10^6, a lift coefficient of 0.30, and a pitching moment coefficient of -0.06. In addition, the airfoil was constrained to be 15% thick with a leading-edge radius of 1.4% chord.

In Figs. 8 and 9, the upper and lower surface N-factor distributions of the NACA 64_1-212 are shown. An N-factor of 13.5 is used in these figures to predict the location where the flow undergoes transition. Because the N-factor distributions of the NACA 64_1-212 are below this transition threshold, this indicates that the boundary-layer solver predicted laminar boundary-layer separation at approximately 50% chord on both surfaces of the airfoil. As a result, the analysis N-factors of this airfoil were artificially extended as described earlier so that the target pressure/N-factor relationship could be used to calculate a target pressure distribution.

The final target N-factor distributions that have been used in the design of the new airfoil are also shown in Figs. 8 and 9. These target N-factor distributions were established to increase the extent of laminar flow over both surfaces. The N-factor distributions of the new airfoil, which are also in Figs. 8 and 9, match the target N-factor distributions very well.

Figure 10 shows a comparison between the pressures of the NACA 64_1-212 and the new airfoil. The pressure distributions of the two airfoils are quite different. The pressure gradient of the new airfoil is more favorable ahead of 30% chord on the upper surface than that of the NACA 64_1-212. In addition, the pressure gradient of the new airfoil is less adverse after 30% chord, which helped maintain laminar flow to 65% chord.

All of the aerodynamic and geometric design constraints have been met in the design of the new airfoil. As a result, the drag coefficient was reduced from 0.0042 for the NACA 64_1-212 to 0.0024 for the new airfoil.

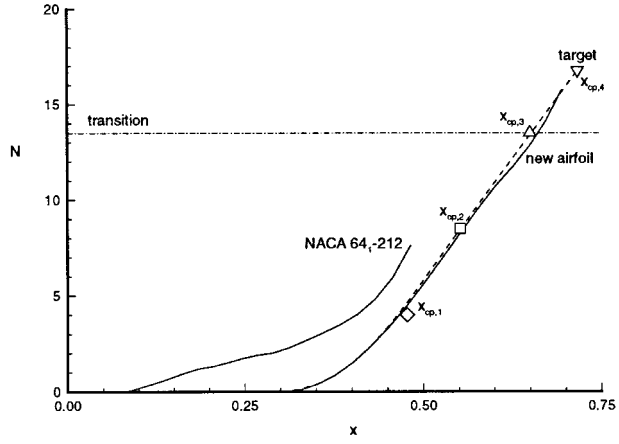

Fig. 8 Comparison of the N-factors on the upper surface of the NACA 64_1-212 and the new airfoil.

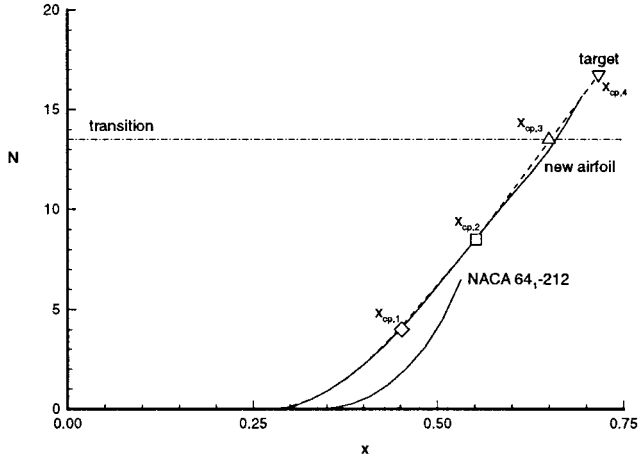

Fig. 9 Comparison of the N-factors on the lower surface of the NACA 64_1-212 and the new airfoil.

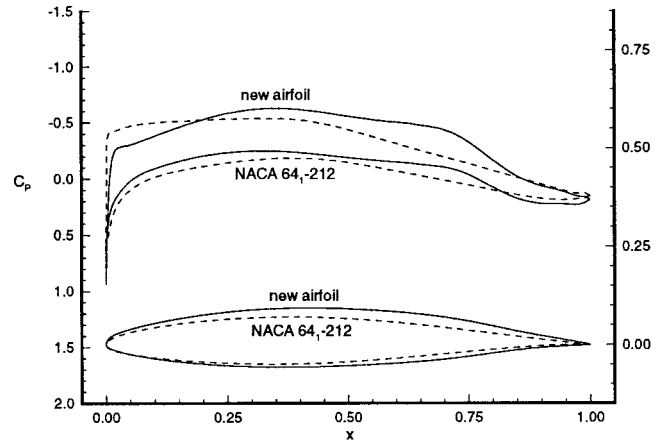

Fig. 10 Comparison of the pressures of the NACA 64_1-212 and the new airfoil at $M = 0.10$, $Re = 3 \times 10^6$, and $c_l = 0.30$.

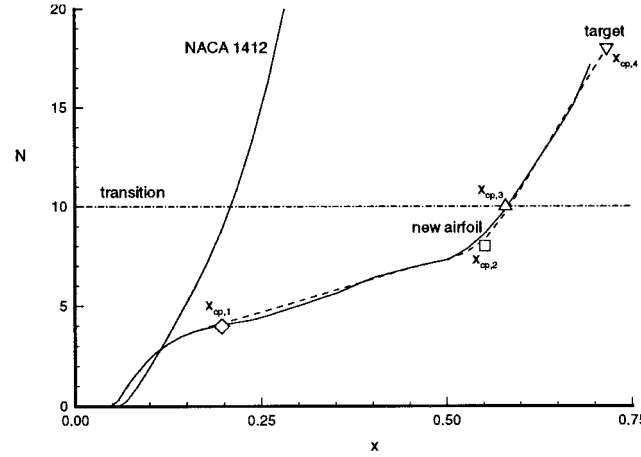

Fig. 11 Comparison of the N-factors on the upper surface of the NACA 1412 and the new airfoil.

Airfoil for a Commuter Aircraft

As the final example, the NACA 1412 airfoil was redesigned to increase the amount of NLF on both surfaces. At a Mach number of 0.60 and a Reynolds number of 2×10^7, the aerodynamic design goals included 60% chord NLF on both surfaces at a lift coefficient of 0.40 and a pitching moment coefficient of -0.08. In addition, the airfoil was constrained to be 12% thick, with a leading-edge radius of 1% chord.

Figures 11 and 12 show the upper and lower surface N-factor distributions of the original NACA 1412 airfoil. Using a transition N-factor of 10, the flow undergoes transition at 20 and 25% chord, respectively, on the upper and lower surfaces. The upper and lower surface N-factor distributions, with the target N-factor distributions, are also plotted in Figs. 11 and 12. The analysis N-factor distributions on both surfaces of the new airfoil are very similar to the target N-factor distributions, which increased laminar flow to 60% chord on both surfaces.

The pressure distributions of the NACA 1412 and the new airfoil are compared in Fig. 13. The adverse pressure gradients seen on the NACA 1412 surface have been replaced with favorable pressure gradients in designing the new airfoil. This is the mechanism by which NLF was achieved in this design. The smaller leading-edge radius of the new airfoil was essential in obtaining the favorable pressure gradients on both surfaces.

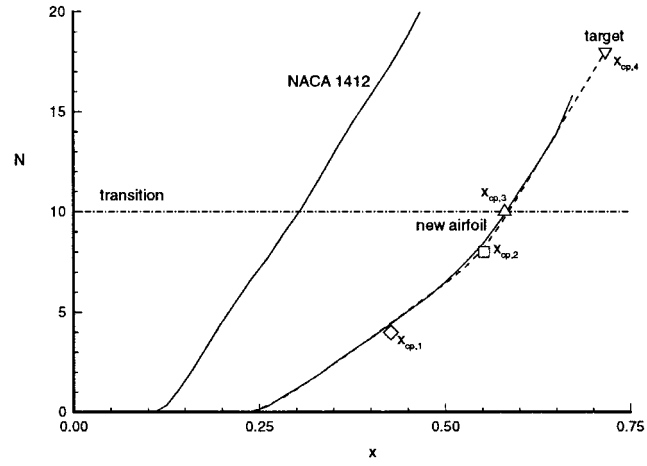

Fig. 12 Comparison of the *N*-factors on the lower surface of the NACA 1412 and the new airfoil.

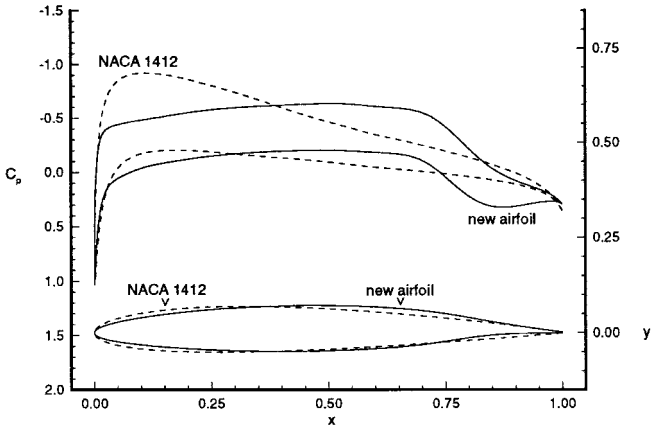

Fig. 13 Comparison of the NACA 1412 and the new airfoil at $M = 0.60$, $Re = 2 \times 10^7$, and $c_l = 0.40$.

In designing this new airfoil, the drag coefficient was reduced from 0.0056 for the NACA 1412 to 0.0028 for the new NLF airfoil.

The current design process could not simultaneously meet all of the design objectives for this airfoil design. In particular, the upper and lower NLF constraints were not being achieved while maintaining both the thickness and leading-edge radius constraints. As a result, the leading-edge radius constraint was eliminated, so that the desired extent of NLF could be achieved on both surfaces. Maintaining the leading-edge radius constraint would have required the maximum thickness of the airfoil to be larger than 12% chord. While maintaining the maximum thickness constraint, the leading-edge radius of the redesigned airfoil was 0.78% chord. All of the other constraints were then satisfied in this design.

Several observations can be made about the design of this new commuter airfoil. First, one does not need to start with an airfoil that has a significant amount of NLF, e.g., the NACA 64_1-212, to design a new airfoil using this method. In addition, this example shows that it can be necessary to release certain geometric constraints to meet the NLF constraints on both surfaces.

General Observations

As mentioned previously, the current method is fully automated and requires four input files to be specified prior to designing a new airfoil. As it currently exists, a Fortran driver program executes the design of a single surface of the airfoil. For two-surface designs, a unix script file is used to successively call the driver program to design each surface.

The success of the method, however, is dependent upon the initial airfoil that is used and the constraints that are implemented. The initial airfoil should have a smooth and continuous pressure distribution. Starting from an airfoil that has a large pressure peak in the leading-edge region is undesirable. In this case, the laminar boundary-layer solver detects laminar separation just aft of the peak and, as a result, the analysis *N*-factors can't be calculated over much of the surface. Moreover, because of the pressures in the leading-edge region, the method for artificially extending the *N*-factors may not work well enough to produce a smooth analysis *N*-factor curve. Even if a smooth curve were obtained, the pressures in the peak region of the initial airfoil would influence the new target pressures and the target pressures may be unreasonable for designing a new airfoil.

In addition, if the constraints are not feasible for laminar flow airfoils, then the method will release one or more of the constraints. For example, requiring an 8% thick airfoil to have a leading-edge radius of 3% chord, as well as laminar flow on both surfaces of the airfoil would result in either the thickness or the leading-edge radius constraint being released. Another option is to release the requirement that the lower surface have laminar flow. User experience is needed to know which way is best for specific problems.

The method is moderately robust, but things do occur that may cause the program to terminate early. For example, the stability analysis code may encounter problems for a given frequency of the Tollmien–Schlichting waves. If this occurs, then the user must change the range of the frequency search within the input file, and execute the program again. In this case, the user may restart the design from the current airfoil.

Concluding Remarks

An automated two-dimensional method has been developed for designing natural laminar flow airfoils while maintaining several other aerodynamic and geometric constraints. The method has been shown to work for a range of Mach numbers, Reynolds numbers, and airfoil thicknesses.

Several existing CFD codes were coupled together modularly to develop this method, which can design natural laminar flow airfoils relatively quickly. To accomplish this, a pressure/*N*-factor relationship was developed to modify target pressures to meet a specified *N*-factor distribution so that an airfoil could be designed to meet a laminar flow constraint, in addition to meeting other aerodynamic and geometric constraints. This method has been used to successfully design a number of airfoils, with results shown for glider, general aviation, and commuter applications.

Acknowledgments

This research was conducted in partial fulfillment of a Master of Science degree with the George Washington University, and was completed at NASA Langley Research Center.

References

[1]Green, B. E., "An Approach to the Constrained Design of Natural Laminar Flow Airfoils," NASA CR-201686, Feb. 1997.

[2]Hartwich, P. M., "Comparison of Coordinate-Invariant and Coordinate-Aligned Upwinding for the Euler Equations," *AIAA Journal*, Vol. 32, No. 9, 1994, pp. 1791–1799.

[3]Hartwich, P. M., "Euler Study on Porous Transonic Airfoils with a View Toward Multipoint Design," *Journal of Aircraft*, Vol. 30, No. 2, 1993, pp. 184–191.

[4]Hartwich, P. M., "Fresh Look at Floating Shock Fitting," *AIAA Journal*, Vol. 29, No. 7, 1991, pp. 1084–1091.

[5]Stratford, B. S., and Beavers, G. S., "The Calculation of the Compressible Turbulent Boundary Layer in an Arbitrary Pressure Gradient—A Correlation of Certain Previous Methods," British Aeronautical Research Council, R&M 3207, Sept. 1959.

[6]Iyer, V., "Computation of Three-Dimensional Compressible Boundary Layers to Fourth-Order Accuracy on Wings and Fuse-

lages,'' NASA CR-4269, Jan. 1990.
[7]Malik, M. R., ''COSAL — A Black-Box Compressible Stability Analysis Code for Transition Prediction in Three-Dimensional Boundary Layers,'' NASA CR-165925, May 1982.
[8]Mack, L. M., ''Boundary-Layer Linear Stability Theory,'' AGARD, Rept. 709, 1984, pp. 3-1–3-81.
[9]Campbell, R. L., ''An Approach to Constrained Aerodynamic Design with Application to Airfoils,'' NASA TP-3260, Nov. 1992.
[10]McGhee, R. J., Viken, J. K., Pfenninger, W., Beasley, W. D., and Harvey, W. D., ''Experimental Results for a Flapped Natural-Laminar-Flow Airfoil with High Lift/Drag Ratio,'' NASA TM-85788, May 1984.
[11]Bauer, F., Garabedian, P., and Korn, D., *A Theory of Supercritical Wing Sections, with Computer Programs and Examples*, Springer–Verlag, New York, 1972.
[12]Bauer, F., Garabedian, P., Korn, D., and Jameson, A., *Supercritical Wing Sections II*, Springer–Verlag, New York, 1975.
[13]Bauer, F., Garabedian, P., and Korn, D., *Supercritical Wing Sections III*, Springer–Verlag, New York, 1977.
[14]Srokowski, A. J., and Orszag, S. A., ''Mass Flow Requirements for LFC Wing Design,'' AIAA Paper 77-1222, Aug. 1977.
[15]Stratford, B. S., ''The Prediction of Separation of the Turbulent Boundary Layer,'' *Journal of Fluid Mechanics*, Vol. 5, Jan. 1959, pp. 1–16.